Design of Oxygen Reduction Bimetallic Catalysts: Ab-Initio-Derived Thermodynamic Guidelines

ARTICLE *in* THE JOURNAL OF PHYSICAL CHEMISTRY B · OCTOBER 2005

Impact Factor: 3.3 · DOI: 10.1021/jp0543779 · Source: PubMed

2 AUTHORS:

Yixuan Wang
Albany State University
55 PUBLICATIONS **1,419** CITATIONS
SEE PROFILE

Perla B. Balbuena
Texas A&M University
245 PUBLICATIONS **5,781** CITATIONS
SEE PROFILE

Design of Oxygen Reduction Bimetallic Catalysts: Ab-Initio-Derived Thermodynamic Guidelines

Yixuan Wang and Perla B Balbuena*

Department of Chemical Engineering, Texas A&M University, College Station, Texas 77843

Received: August 5, 2005

The Gibbs free energies of key elementary steps for the electrocatalytic oxygen reduction reaction (ORR) are calculated with B3LYP type of density functional theory: $O_2 + M + H^+ + e^-$ (0 eV) → HOO−M (ΔG_1), HOO−M + M → HO−M + O−M (ΔG_2), $O_2 + 2M + H^+ + e^-$ (0 eV) → O−M + HO−M (ΔG_3), and HO−M + O−M + $3H^+ + 3e^-$ (0 eV) → $2H_2O$ + 2M (ΔG_4), where H^+ is modeled as $H_3^+O(H_2O)_3$ and M stands for the adsorption site of a metal catalyst modeled by a single metal atom as well as by an M_3 cluster. Taking Pt as a reference, ΔG_4 is plotted against ΔG_1 for 17 metals from groups V to XII. It is found that no single metal has both ΔG_1 and ΔG_4 more negative than Pt, although some of them have either more negative ΔG_1 or more negative ΔG_4. This enables us to explain thermodynamically why no other single metal catalyzes the ORR as effectively as Pt does. Moreover, a thermodynamic analysis reveals that the signs of $\Delta\Delta G$ (the difference between ΔG of other metals and ΔG of Pt) strongly correlate with the valence electronic structure of metals, i.e., $\Delta\Delta G_1 < 0$ and $\Delta\Delta G_4 > 0$ for metals M with vacant valence d orbitals, whereas $\Delta\Delta G_1 > 0$ and $\Delta\Delta G_4 < 0$ for metals M′ with fully occupied valence d orbitals. Thus, a simple thermodynamic rule for the design of bimetallic catalysts for the ORR is proposed: couple a metal M ($\Delta\Delta G_1 < 0$) with a second metal M′ ($\Delta\Delta G_4 < 0$) to form an alloy catalyst MM'_3. The rationale behind this selection is based on M being more efficient for the rate-determining step, i.e., for the formation of the adsorbed species M−OOH, while M′ can enhance the reductions of O and OH in the last three electron-transfer steps.

Introduction

The oxygen reduction reaction (ORR) on Pt and Pt alloys is being intensely scrutinized[1−14] due to the strong interest associated with the search of efficient cathode catalysts for low-temperature fuel cells. Suggested mechanisms for the ORR in acidic media could be generally classified into two main groups: a *direct* four-electron pathway where O_2 is initially dissociatively chemisorbed, with the O═O bond cleavage leading to adsorbed oxygen radicals, which are then reduced directly to water,[15] and a *series* pathway involving the formation of superoxide ion ($O_2^{\bullet -}$) in the first electroreduction step,[16] or hydrogen peroxide H_2O_2, which will decompose or be reduced to water. Despite extensive research, the mechanisms for the ORR still remain highly controversial, even on poly-Pt crystalline surfaces.[17,18]

Using ab-initio molecular dynamics, an alternative reaction pathway for the ORR on Pt(111) was suggested by us.[19] It was theoretically validated that the O_2 reduction on a Pt surface may proceed via a *parallel* pathway, the direct and series occurring simultaneously, with the direct as the dominant step. The adsorption of O_2 and electron transfer in eq 1a are strongly coupled. In line with the suggestions from Damjanovic[20] and Anderson's group,[6] a proton was found to participate in the first electroreduction step. In addition, the proton transfer cooperates with the electron transfer in eq 1b, resulting in the formation of an adsorbed radical OOH, HOO−M. The elementary step in eq 1b could be considered as a rate-determining step (rds), and the energy barrier is approximately 0.4 eV. Nevertheless, no clear barrier exists in the dissociation of HOO−M (eq 2), in agreement with previous reports.[6]

$$O_2 + M + \delta e^- \rightarrow OO^{\delta -}-M \quad (1a)$$

$$OO^{\delta -}-M + H^+ + (1-\delta)e^- \rightarrow HOO-M \quad (1b)$$

$$O_2 + M + H^+ + e^- \rightarrow HOO-M \quad (\Delta G_1) \quad (1)$$

$$HOO-M + M \rightarrow HO-M + O-M \quad (\Delta G_2) \quad (2)$$

The reaction for the first electron reduction is

$$O_2 + 2M + H^+ + e^- \rightarrow O-M + HO-M \quad (\Delta G_3) \quad (3)$$

Here, M represents an adsorption site of a metal surface. For the rest of the electroreductions, adsorbed O and OH would be reduced to waters that eventually need to be desorbed from the metal surface. Independently of the details, the overall reaction for the subsequent three electron and proton transfers would be

$$HO-M + O-M + 3H^+ + 3e^- \rightarrow 2H_2O + 2M \quad (\Delta G_4) \quad (4)$$

In the present investigation, thermodynamic properties, especially Gibbs free energies of eq 1 (ΔG_1), eq 2 (ΔG_2), and eq 4 (ΔG_4), are carefully calculated with density functional theory in order to obtain new insights into the ORR on transition metals and to eventually suggest a guideline for rational design of new catalysts for the ORR.

Computational Details

Seventeen single atoms from groups V to XII as well as M_3 clusters for 10 of them are used to model adsorption sites, and

* Corresponding author. E-mail: balbuena@tamu.edu.

10.1021/jp0543779 CCC: $30.25
Published on Web 09/17/2005

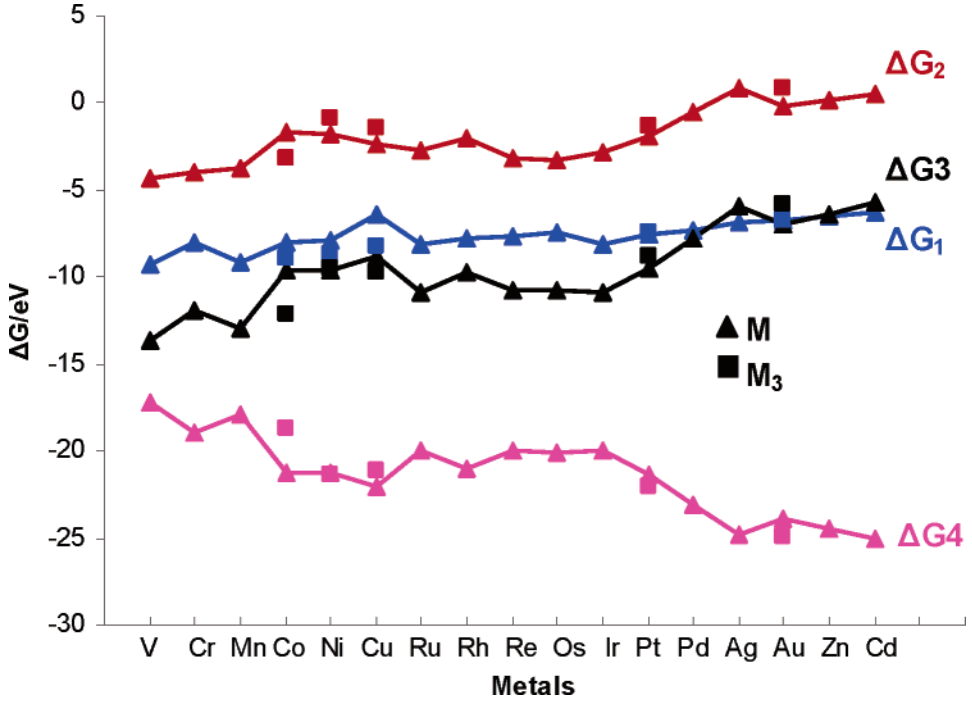

Figure 1. Gibbs free energy variations (ΔG, eV) for eqs 1−4, calculated with B3LYP/LANL2DZ +6-311++G**.

a solvated proton is modeled by $H_3O^+(H_2O)_3$. In each case the electron was given an energy of zero that corresponds to zero cell potential ($U = 0$ V). Geometries are fully optimized with the hybrid B3LYP density functional[21,22] as implemented in Gaussian03 Rev C.02[23] together with the LANL2DZ pseudopotential and the corresponding double-ζ basis set for Pt[24] and with 6-311++G** for oxygen and hydrogen. A quadratically convergent SCF procedure and ultrafine integration are employed. To characterize stationary points and make estimations such as thermal and entropic contributions to the free energy, frequency analyses are done for all stationary points at the same theory level as the geometry optimizations. Many different geometric structures and electronic and spin states are usually found for the present species with open shell electronic structures, yet only the ground state for certain species is used to calculate ΔG at 298.2 K.

The reaction free energies are based on the hydronium model, $H_3O^+(H_2O)_3$. One therefore needs to use its free energy to compute ΔG of a given reaction; for instance, eq 1 can be written like

$$O_2 + M + H_3O + (H_2O)_3 + e^- \rightarrow HOO{-}M + (H_2O)_4 \quad (1')$$

$$\Delta G_1 = G[(H_2O)_4] + G(HOO{-}M) - G(O_2) - G(M) - G[H_3O^+(H_2O)_3] - U(e)$$

where $U(e) = 0$ V and $G(M)$ is the Gibbs free energy of either metal atom or metal cluster.

Thermodynamic Diagram. Both slab and cluster models are being widely used as models of metal surfaces for relevant theoretical DFT investigations of the ORR.[9−11,13,14,25] To get energetic predictions in agreement with experiments done on surfaces, clusters with 28 or more atoms might be required.[14] However, clusters as small as Pt_2 or even a single Pt atom can provide reasonable energetic estimates of binding energies of metal oxides on extended Pt surfaces.[6,26] Conventional DFT methods are unable to properly describe uncoordinated O_2^- mainly because of its multielectronic configuration character,[27] which requires more sophisticated electronic structure methods such as MRCI or CCSD(T). However, for bounded oxides on metal surface DFT methods are proper and have been validated by agreement with experiments.[6,26,28] Moreover, since the focus of our current interest is to obtain energetic differences rather than absolute magnitudes for the ORR on a variety of metal surfaces, the present models of single M and M_3 and the applied B3LYP method also can cancel systematic errors to some extent, thus yielding valuable information.

Figure 1 shows that the Gibbs free energy values from the single atoms (triangles) are in good agreement with the available data obtained with the M3 clusters (squares). According to Figure 1, values of the formation Gibbs free energy of HOO−M (ΔG_1, eq 1) for the various M elements are basically parallel to those of its dissociation free energy (ΔG_2, eq 2). Since both pathways are driven by chemisorption of oxides like OOH for eq 1 and O and OH for eq 2 via M−O bonds, the metals that favor the formation of M−OOH will also enhance O−O bond cleavage by stabilizing M−O and M−OH. ΔG_3, the sum of ΔG_1 and ΔG_2, corresponding to the reversible potential on the physical scale for the first electroreduction of O_2, is also given in Figure 1. The cumulative change of Gibbs free energy (ΔG_4, eq 4) for the rest of the electron reduction steps varies in an opposite way to ΔG_1. That means that the strong stability of the M−O and M−OH bonds (high negative ΔG_1) will not favor reductions of O and OH groups, resulting in a less negative ΔG_4.

Assuming that the ORR involves an initial dissociative chemisorption, eq 5, followed by the four-electron reduction of the oxide in eq 6

$$O_2 + 2M \rightarrow 2MO \quad (5)$$

$$2MO + 4H^+ + 4e^- \rightarrow 2H_2O + 2M \quad (6)$$

Bard et al.[17] recently reported the variation of the Gibbs free energy for reaction 5 vs the standard reduction potential for reaction 6 for approximately 11 metals and proposed a thermodynamic guideline for the design of electrocatalysts for the ORR. Inspired by Bard et al.'s ideas, and in view of the

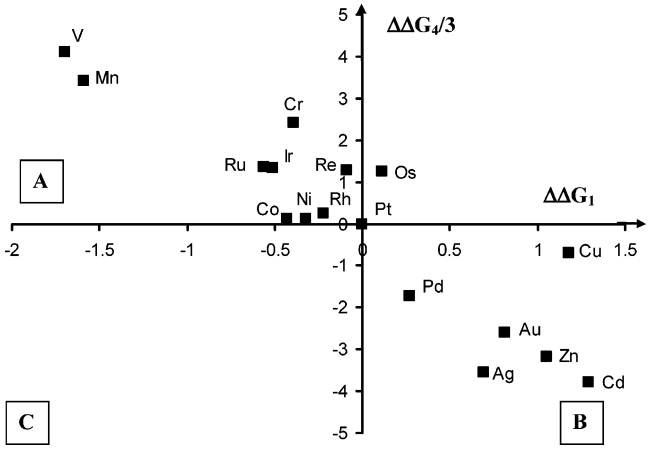

Figure 2. Plot of relative Gibbs free energies (eV), $\Delta\Delta G_4/3$ vs $\Delta\Delta G_1$. The metals (M) in region A have vacant valence d orbitals and are able to more efficiently enhance thermodynamically the formation of M−OOH, whereas the valence d orbitals for the metals (M′) in region B are fully occupied and the metals M′ favor the reductions of M−O and M−OH.

fact that Pt is still the best catalyst known for the ORR, we have taken Pt as a reference to plot ΔG_4 for the last three electron-transfer steps (eq 4) against ΔG_1 for the rate-determining step (eq 1), as shown in Figure 2. The diagram clearly shows the ability of the various metals to thermodynamically facilitate the rds (formation of M−OOH) and the rest of the ORR as compared with Pt. $\Delta\Delta G_n$ ($n = 1, 4$) in Figure 2 was defined as

$$\Delta\Delta G_n = \Delta G_n(\mathrm{M}) - \Delta G_n(\mathrm{Pt}) \qquad (7)$$

In the upper left quadrant of Figure 2 (region A), metals favor thermodynamically the formation of M−OOH ($\Delta\Delta G_1 < 0$) by stabilizing chemisorption of OOH, while positive $\Delta\Delta G_4$ indicates that the reductions of O and OH are unfavorable on the surface of these metals because of too strong adsorptions of O and OH groups. The metals in the lower right quadrant (region B) have opposite performance. According to thermodynamics, both ΔG_1 and ΔG_4 for a given metal should be more negative than those corresponding to Pt, in order for that metal to be a better candidate than Pt to catalyze the ORR, i.e., $\Delta\Delta G_1$ and $\Delta\Delta G_4 < 0$. Unfortunately, none appears in the lower left quadrant (region C). Thus, although the origin of the Pt success catalyzing the ORR is uncertain, Figure 2 unambiguously explains from a thermodynamics point of view why no any other monometal catalyzes the ORR as effectively as Pt does.[29]

The results arising from the above thermodynamic analysis somewhat fulfill the Sabatier principle of catalysis, which states that the catalytic activity for a given reaction follows a volcano curve through the periodic table because an intermediate degree of binding of reaction intermediates to the surface will give an optimal catalyst.[30] For example, Figure 2 shows that Pt is the best catalyst for the ORR from a thermodynamic viewpoint. Applying the concept of Sabatier analysis, Norskov et al. have shown an interesting volcano plot for oxygen reduction activity as a function of the oxygen binding energies of O or OH.[9] The regions A and B in Figure 2 roughly correspond to the two sides in Norskov's volcano.

It should be stressed that the revealed information in Figure 2 arises from thermodynamic properties for eqs 1 and 4; it is well-known that the performance of the metals as the catalysts of the ORR is eventually dependent on their kinetic factors like activation barriers. Further investigations into kinetic behavior of the important reaction are also very necessary.

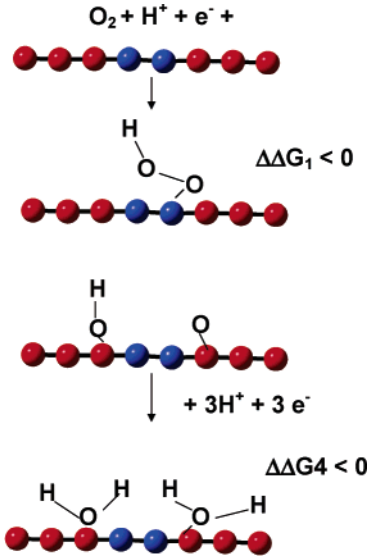

Figure 3. Scheme of the proposed thermodynamic guideline, showing the M atoms (blue) favoring OOH formation and the M′ atoms (red) favorable to O and OH reduction.

Strong Correlation between $\Delta\Delta G$ and Electronic Structure. Close inspection of Figure 2 indicates that all of the metals in region A have vacant valence d orbitals, whereas valence d orbitals for the metals in region B are fully occupied. This means that the signs of $\Delta\Delta G$ are in strong correlation with the valence electronic structure of the transition metals. As previously speculated,[31] Figure 2 clearly shows that vacant d orbitals play a very important role in the rds of the ORR. Meanwhile, it is noticed that the metals with high negative $\Delta\Delta G_1$ give rise to high positive $\Delta\Delta G_4$, decreasing the reduction potential of M−O and M−OH, e.g., V and Mn. According to this correlation, it can be concluded that metals with vacant valence d orbitals in area A could only enhance the first reduction step ($\Delta\Delta G_1 < 0$) and that metals with fully occupied d orbitals in area B increase the reduction potential for the last three reductions ($\Delta\Delta G_4 < 0$).

Implication to the Design of Alloy Catalysts: An ab-Initio Thermodynamic Guideline. Figure 2 and the above correlation enable us to propose a thermodynamic guideline for the design of alloy catalysts for the ORR. To constitute Pt-based bimetallic systems, it is proper to find another metal (M) within a limited range, e.g., -0.5 eV $< \Delta\Delta G_1, \Delta\Delta G_4 < 0.5$ eV, where eight metals M (Co, Ni, Pd, Rh, Re, Ru, Ir, and Os) have reduction potentials similar to Pt. In fact, a few bimetallics such as Pt−Ni and Pt−Co have already been well established as good catalysts for the ORR.[18] Thus, following Bard et al., [17] a thermodynamic guideline could be suggested as follows: couple a metal M in region A ($\Delta\Delta G_1 < 0$) with another metal M′ in region B ($\Delta\Delta G_4 < 0$) to form alloy catalysts MM'_3. Thus, both $\Delta\Delta G_1$ and $\Delta\Delta G_4$ will be less than zero for the bimetallic alloy, and the composition (1:3) from experiments[4] may relate to the fact that more electron reductions will occur on M′, thus requiring more M′ sites. According to the proposed guideline, $\Delta\Delta G_1 < 0$ and $\Delta\Delta G_4 = 0$ for the already defined bimetallic systems such as $NiPt_3$ and $CoPt_3$. Thus, the rds (formation of M−OOH) may be more efficiently catalyzed by the two alloys as compared with pure poly-Pt. Figure 3 further sketches how the guideline works. The first electroreduction takes place on metal M from region A ($\Delta\Delta G_1 < 0$), e.g., Ni, Co, Ru, etc., forming M−OOH followed by a spontaneous dissociation into

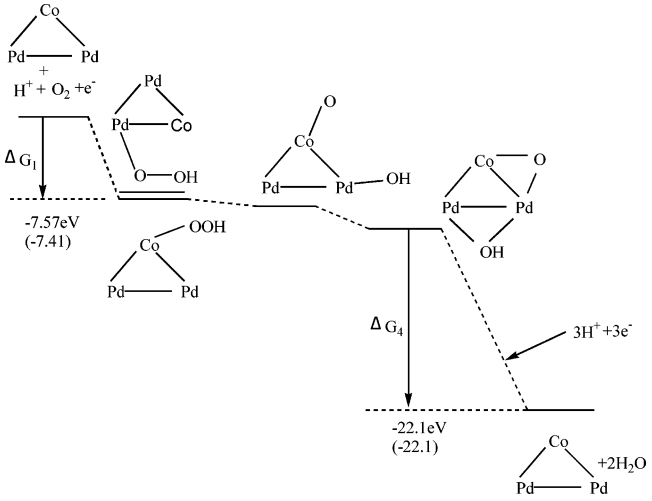

Figure 4. Gibbs free energy profile for the ORR on Pd_2Co. The data in parentheses are for Pt_3. Pd_2Co is expected to have slightly better performance than Pt_3 by favoring the first electroreduction step.

O and OH, which then will diffuse to 2-fold or 3-fold sites made of metal M′. The reductions of O and OH on M′ sites cause $\Delta\Delta G_4 < 0$.

The combination Pd_4Co that has recently been shown to exhibit high activity for the ORR[17,32] satisfies the proposed principle. The Gibbs energy profile for the ORR on Pd_2Co is illustrated in Figure 4. As expected, one-end chemisorption of OOH on Co is the most stable of a variety of OOH adsorptions on Pd_2Co. The bridge adsorption species is more stable than atop adsorptions of O and OH, which may drive their diffusion following the decomposition of $Pd_2Co-OOH$. The ΔG_1 of Pd_2Co is ~0.15 eV more negative than that of Pt_3, while ΔG_4 is almost the same as those of Pd_2Co and Pt_3. Thus, the bimetallic system thermodynamically has similar performance to Pt to catalyze the ORR.

It should be mentioned that the above discussion for alloy catalysts design assumes that both components are always on the surface with the composition of MM'_3. However, the surface can be enriched by one of the components; i.e., surface segregation may occur[33,34] in some practical cases, such as $Pt_{75}Ni_{25}$, in which the Pt atoms are enriched in the outermost and third atomic shells while the Ni atoms are enriched in the second atomic shell.[35] Moreover, details of surface segregation depend on particle size, shape, preparation, and substrate[36,37] and even on the presence of adsorbates and solvent.[38] The interactions between Ni atoms in the second shell and surface Pt atoms may change the geometric structure (e.g., Pt−Pt distance) and electronic structure (energy levels of the frontier orbitals) so that $\Delta\Delta G_1$ and/or $\Delta\Delta G_4$ become negative; i.e., the thermodynamic activity of the alloy for the ORR is enhanced. How to accurately explain these detailed interactions resulting in better ORR catalysts needs to be further studied.

Conclusion. Density functional theory was employed to investigate the thermodynamics of key steps of the electrocatalytic oxygen reduction reaction (ORR), such as the formation of OOH (ΔG_1) and the reductions of O and OH (ΔG_4). It was found that no single metal yields both ΔG_1 and ΔG_4 more negative than Pt. This enables us to explain thermodynamically why no any other single metal catalyzes the ORR as effectively as Pt does. The plot of ΔG_4 against ΔG_1 for 17 metals from group V to XII has two interesting quadrants, the upper left ($\Delta\Delta G_1 < 0$ and $\Delta\Delta G_4 > 0$) and the lower right ($\Delta\Delta G_1 > 0$ and $\Delta\Delta G_4 < 0$), which strongly correlate with the valence electronic structure of metals; i.e., the metals M in the upper left quadrant have vacant valence d orbitals, whereas the metals M′ in the lower right quadrant have fully occupied valence d orbitals. Moreover, a thermodynamic guideline for the design of bimetallic catalysts for the ORR is proposed: coupling a metal M ($\Delta\Delta G_1 < 0$) with a second metal M′ ($\Delta\Delta G_4 < 0$) to form an alloy catalyst MM'_3 can enhance not only the first electroreduction step but also the other three reduction steps.

Acknowledgment. Financial support from the Department of Energy/Basic Energy Sciences (DE-FG02-04ER15619) and from DURIP/ARO (Grant W911N F-04-1-0098) is gratefully acknowledged. The use of computational facilities at the NSF HPC and TeraGrid Sites: National Center for Supercomputing Applications (CHE040052) is appreciated.

References and Notes

(1) Damjanovic, A.; Brusic, V. Electrode kinetics of oxygen reduction on oxide-free platinum electrodes. *Electrochim. Acta* **1967**, *12*, 615−628.

(2) Yeager, E. B. Electrocatalysts for O_2 reduction. *Electrochim. Acta* **1984**, *29*, 1527−1537.

(3) Adzic, R. Recent advances in the kinetics of oxygen reduction. In *Electrocatalysis*; Lipkowski, J., Ross, P. N., Eds.; Wiley-VCH: New York, 1998; pp 197−242.

(4) Markovic, N. M.; Ross, P. N. Surface Science Studies of Model Fuel Cells Electrocatalysts. *Surf. Sci. Rep.* **2002**, *45*, 117−229.

(5) Anderson, A. B.; Albu, T. V. Catalytic effect of platinum on oxygen reduction: An ab initio model including electrode potential dependence. *J. Electrochem. Soc.* **2000**, *147*, 4229−4238.

(6) Sidik, R. A.; Anderson, A. B. Density functional theory study of O_2 electroduction when bonded to a Pt dual site. *J. Electroanal. Chem.* **2002**, *528*, 69−76.

(7) Xu, Y.; Ruban, A. V.; Mavrikakis, M. Adsorption and dissociation of O_2 on Pt−Co and Pt−Fe alloys. *J. Am. Chem. Soc.* **2004**, *126*, 4717−4725.

(8) Murthi, V. S.; Urian, R. C.; Mukerjee, S. Oxygen reduction kinetics in low and medium-temperature acid environment: Correlation of water activation and surface properties in supported Pt and Pt alloy electrocatalysts. *J. Phys. Chem. B* **2004**, *108*, 11011−11023.

(9) Norskov, J. K.; Rossmeisl, J.; Logadottir, A.; Lindqvist, L.; Kitchin, J. R.; Bligaard, T.; Jonsson, H. Origin of the overpotential for oxygen reduction at a fuel-cell cathode. *J. Phys. Chem. B* **2004**, *108*, 17886−17892.

(10) Panchenko, A.; Koper, M. T. M.; Shubina, T. E.; Mitchell, S. J.; Roduner, E. Ab Initio Calculations of Intermediates of Oxygen Reduction on Low-Index Platinum Surfaces. *J. Electrochem. Soc.* **2004**, *151*, A2016−A2027.

(11) Balbuena, P. B.; Altomare, D.; Vadlamani, N.; Bingi, S.; Agapito, L. A.; Seminario, J. M. Adsorption of O, OH, and H_2O on Pt-based bimetallic clusters alloyed with Co, Cr, and Ni. *J. Phys. Chem. A* **2004**, *108*, 6378−6384.

(12) Seminario, J. M.; Agapito, L. A.; Yan, L.; Balbuena, P. B. Density functional theory study of adsorption of OOH on Pt-based bimetallic clusters alloyed with Cr, Co, and Ni. *Chem. Phys. Lett.* **2005**, *410*, 275−281.

(13) Kitchin, J. R.; Norskov, J. K.; Barteau, M. A.; Chen, J. G. Modification of the surface electronic and chemical properties of Pt(111) by subsurface 3 d transition metals. *J. Chem. Phys.* **2004**, *120*, 10240−10246.

(14) Jacob, T.; Muller, R. P.; W. A. Goddard, I. Chemisorption of Atomic Oxygen on Pt(111) from DFT Studies of Pt−Clusters. *J. Phys. Chem. B* **2003**, *107*, 9465−9476.

(15) Clouser, S. J.; Huang, J. C.; Yeager, E. B. Temperature dependence of the Tafel slope for oxygen reduction on platinum in concentrated phosphoric acid. *J. Appl. Electrochem.* **1993**, *23*, 597−605.

(16) Markovic, N. M.; Schmidt, T. J.; Stamenkovic, V.; Ross, P. N. Oxygen reduction reaction on Pt and Pt bimetallic surfaces: A selective review. *Fuel Cells* **2001**, *1*, 105−116.

(17) Fernandez, J. L.; Walsh, D. A.; Bard, A. J. Thermodynamic Guidelines for the Design of Bimetallic Catalysts for Oxygen Electroreduction and Rapid Screening by Scanning Electrochemical Microscopy. M-Co (M: Pd, Ag, Au). *J. Am. Chem. Soc.* **2005**, *127*, 357−365.

(18) Stamenkovic, V.; Grgur, B. N.; Ross, P. N.; Markovic, N. M. Oxygen reduction reaction on Pt and Pt-bimetallic electrodes covered by CO−Mechanism of the air bleed effect with reformate. *J. Electrochem. Soc.* **2005**, *152*, A277−A282.

(19) Wang, Y.; Balbuena, P. B. Ab initio Molecular Dynamics Simulations of the Oxygen Electroreduction Reaction on a Pt(111) Surface in the Presence of Hydrated Hydronium (H_3O) + (H_2O)$_2$: Direct or Series Pathway? *J. Phys. Chem. B* **2005**, *109*, 14896−14907.

(20) Damjanovic, A.; Sepa, D. B.; Vojnovic, M. V. New evidence supports the proposed mechanism for dioxygen reduction at oxide free platinum electrodes. *Electrochim. Acta* **1979**, *24*, 887−889.

(21) Becke, A. D. A new mixing of Hartree−Fock and local density-functional theories. *J. Chem. Phys.* **1993**, *98*, 1372−1377.

(22) Lee, C.; Yang, W.; Parr, R. G. Development of the Colle-Salvetti correlation-energy formula into a functional of the electron density. *Phys. Rev. B* **1988**, *37*, 785−789.

(23) Frisch, M. J.; Trucks, G. W.; Schlegel, H. B.; Scuseria, G. E.; Robb, M. A.; Cheeseman, J. R.; Montgomery, J. A.; Vreven, T.; Kudin, K. N.; Burant, J. C.; Millam, J. M.; Iyengar, S. S.; Tomasi, J.; Barone, V.; Mennucci, B.; Cossi, M.; Scalmani, G.; Rega, N.; Petersson, G. A.; Nakatsuji, H.; Hada, M.; Ehara, M.; Toyota, K.; Fukuda, R.; Hasegawa, J.; Ishida, M.; Nakajima, T.; Honda, Y.; Kitao, O.; Nakai, H.; Klene, M.; Li, X.; Knox, J. E.; Hratchian, H. P.; Cross, J. B.; Bakken, V.; Adamo, C.; Jaramillo, J.; Gomperts, R.; Stratmann, R. E.; Yazyev, O.; Austin, A. J.; Cammi, R.; Pomelli, C.; Ochterski, J. W.; Ayala, P. Y.; Morokuma, K.; Voth, G. A.; Salvador, P.; Dannenberg, J. J.; Zakrzewski, V. G.; Dapprich, S.; Daniels, A. D.; Strain, M. C.; Farkas, O.; Malick, D. K.; Rabuck, A. D.; Raghavachari, K.; Foresman, J. B.; Ortiz, J. V.; Cui, Q.; Baboul, A. G.; Clifford, S.; Cioslowski, J.; Stefanov, B. B.; Liu, G.; Liashenko, A.; Piskorz, P.; Komaromi, I.; Martin, R. L.; Fox, D. J.; Keith, T.; Al-Laham, M. A.; Peng, C. Y.; Nanayakkara, A.; Challacombe, M.; Gill, P. M. W.; Johnson, B.; Chen, W.; Wong, M. W.; Gonzalez, C.; Pople, J. A. *Gaussian03*, Revision C.02 ed.; Gaussian, Inc.: Wallingford, CT, 2004.

(24) Wadt, W. R.; Hay, P. J. Ab initio effective core potentials for molecular calculations. Potentials for main group elements Na to Bi. *J. Chem. Phys.* **1985**, *82*, 284−298.

(25) Balbuena, P. B.; Calvo, S. R.; Lamas, E. J.; Seminario, J. M. Adsorption and dissociation of H_2O_2 on Pt_3, Pt_2M, PtM_2 (M = Cr, Co, and Ni), Pt(111), and Pt_3Co(111). *J. Phys. Chem. B*, submitted for publication.

(26) Li, T.; Balbuena, P. B. Computational studies of the interactions of oxygen with platinum clusters. *J. Phys. Chem. B* **2001**, *105*, 9943−9952.

(27) Stampfuss, P.; Wenzel, W. Accurate multireference calculations of the electron affinity of NO, BO, and O^{2-}. *Chem. Phys. Lett.* **2003**, *370*, 478−484.

(28) Eichler, A.; Hafner, J. Molecular precursors in the dissociative adsorption of O_2 on Pt (111). *Phys. Rev. Lett.* **1997**, *79*, 4481−4484.

(29) Markovic, N. M.; Ross, P. N. Electrocatalysts by design: from the tailored surface to a commercial catalyst. *Electrochim. Acta* **2000**, *45*, 4101−4115.

(30) Bligaard, T.; Norskov, J. K.; Dahl, S.; Matthiesen, J.; Christensen, C. H.; Sehested, J. The Bronsted-Evans-Polanyi relation and the volcano curve in heterogeneous catalysis. *J. Catal.* **2004**, *224*, 206−217.

(31) Appleby, A. J. Oxygen Reduction on Oxide-Free Platinum in 85% Orthophosphoric Acid: Temperature and Impurity Dependence. *J. Electrochem. Soc.* **1970**, *117*, 328−335.

(32) Savadogo, O.; Lee, K.; Oishi, K.; Mitsushima, S.; Kamiya, N.; Ota, K.-I. New palladium alloys catalyst for the oxygen reduction reaction in an acid medium. *Electrochem. Commun.* **2004**, *6*, 105−109.

(33) Ruban, A. V.; Skriver, H. L.; Norskov, J. K. Surface segregation energies in transition-metal alloys. *Phys. Rev. B* **1999**, *59*, 15990−16000.

(34) Mainardi, D. S.; Balbuena, P. B. Surface Segregation in Bimetallic Nanoclusters: Geometric and Thermodynamic Effects. *Int. J. Quantum Chem.* **2001**, *85*, 580−591.

(35) Wang, G.; VanHove, M. A.; Ross, P. N.; Baskes, M. I. Monte Carlo simulations of segregation in Pt−Ni catalyst nanoparticles. *J. Chem. Phys.* **2005**, *122*, 024706−024712.

(36) Huang, S.-P.; Balbuena, P. B. Melting of bimetallic Cu−Ni nanoclusters. *J. Phys. Chem. B* **2002**, *106*, 7225−7236.

(37) Huang, S.-P.; Mainardi, D. S.; Balbuena, P. B. Structure and dynamics of graphite-supported bimetallic nanoclusters. *Surf. Sci.* **2003**, *545*, 163−179.

(38) Greeley, J.; Mavrikakis, M. Alloy catalysts designed from first principles. *Nat. Mater.* **2004**, *3*, 810−815.